Chapter 3

Segmentation of the Visible Human for High Quality Volume based Visualization

Thomas Schiemann, Ulf Tiede, Karl Heinz Höhne
Institute of Mathematics and Computer Science in Medicine (IMDM)
University Hospital Hamburg-Eppendorf, Germany
e-mail: schiemann@uke.uni-hamburg.de

Abstract

This article describes a combination of interactive classification and super-sampling visualization algorithms that greatly enhances the realism of 3D reconstructions of the Visible Human data sets. Objects are classified on basis of ellipsoidal regions in RGB-space. The ellipsoids are used for super-sampling in the visualization process.

3.1 Introduction

Segmentation is the core problem for many applications in medical imaging. Although it has been worked on by numerous authors for many years, general solutions are not at hand. If we confine ourselves to specific classes of images and to special objectives, however, successful applications can be developed.

In the case of the Visible Human data sets [54] we have three-parametric photographic images, which we want to display in three dimensions using techniques of volume visualization. In the special case of volume visualization from cross-sectional images, it is well known that best visualization results are obtained if the segmentation procedure offers results that ensure smooth coherence of the surface voxels at positions of high intensity gradients. For scalar images (like CT or MRI) this condition is fulfilled if threshold based methods are used [57], because in this case the visualization procedure (ray-casting) can locate surface positions and orientations with sub-voxel resolution resulting in images that show the even smallest structures in a natural way [36, 40]. Other segmentation techniques, which are tailored for other purposes, neglect this coherence and hence often lead to visualization artifacts when small details are to be rendered.

For the color images of the Visible Human Project this paper therefore presents an approach, which generalizes the threshold ranges in scalar space to volumes in RGB-space, which can again build a basis for super-sampled ray-casting. This paper is to demonstrate, that photographic images such as those of the Visible Human can be segmented in a way that delivers realistic images of unprecedented quality.

3.2 Method

3.2.1 Image preprocessing

For our experiments, we worked with the Visible Human male. The data are transverse cross-sectional photographic images of a frozen male cadaver with a resolution of 0.33 mm and slice distance of 1 mm. The images are supplemented by two sequences of high-resolution CT images from the fresh and frozen cadaver with resolutions between approx. 0.5 mm and 1.0 mm and slice distances of 1 mm for the frozen and between 1 mm and 5 mm for the fresh cadaver. The fresh cadaver has also been scanned by MRI, resulting in separated stacks of (mainly coronal) images, which have been obtained with three acquisition protocols (T1, T2, PD). The MR images have lower resolution between 1 mm and 2 mm and slice distances up to 5 mm.

Before acquisition of the photographic images, the cadaver was cut up into different portions. This procedure leads to some shift artifacts in the resulting volume, which are visible as horizontal lines on 3D renderings.

Next to algorithmic problems, which will be addressed later, one of the main difficulties in working with the Visible Human data is their huge size, especially that of the anatomical data. Handling of even small parts of the body in full resolution requires very large disk storage and computer main memory (e.g. 440 M-byte for the raw data of the head alone or 1100 M-byte for the upper abdomen). We have thus reduced the resolution of the anatomical images to 1 mm^3 by averaging 3×3 pixels on every slice. While this procedure has the advantage that the resulting data (49 M-byte for the head or 121 M-byte for the abdomen) can be processed in high-end workstations, it also introduces new segmentation problems, because partial volume effects are created or much enhanced by the averaging procedure.

A 3D scatter-plot of the color distribution of the anatomical images shows that the components are highly correlated. We therefore considered the possibility of reducing the RGB-data into 2-channel data by principal components analysis. But we did not ultimately choose this procedure, since the original colors of the anatomical images are still needed for later interactive segmentation and thus cannot be replaced by the artificial 2-channel data.

The CT and MRI data are roughly registered with the anatomical data. We improved this registration using an interactive landmark-based tool [47]. The main mapping parameters which had to be refined were translation and scaling within the slices. The other parameters (scaling and translation perpendicular to the slices and rotation) were already correct. The registration error is reduced to approx. 1 voxel for the frozen CT dataset, but for the images obtained from the fresh cadaver, locally larger registration errors occur due to morphological changes caused by freezing. The registration procedure allows us to create combined renderings of different modalities in a single view with object parameters split onto the different modalities.

3.2.2 Volume based visualization

For the task of 3D visualization of volume data, there are in general three different approaches [27]:

Rendering of surfaces, which are represented as polygons. In a preprocessing step such as the Marching Cubes algorithm [32], polygons are extracted from the image volume. These surfaces can then

be visualized with standard graphics packages.

Volume rendering produces 3D images by summing up all voxel values along the path of each ray [30, 12]. Different weighting factors, which usually depend on intensity or gradient magnitude, can be assigned to each voxel in order to enhance the appearance of certain objects.

Volume-based rendering of surfaces uses object membership attributes for each voxel during ray-casting in order to decide which voxels are to be rendered and how the rendering shall be performed (e.g. opaque or transparent, shading parameters, etc.) [57]. The membership attributes are obtained from segmentation, which has to be done in advance.

While polygonal surface rendering has the advantage of being fast, if the number of polygons is kept low, considerable detail is usually lost during the preprocessing steps necessary for generating the surfaces. Accurate mapping of surface texture and realistic cutting are difficult to implement. On the other hand pure volume rendering is usually very slow on standard hardware and is generally not capable of creating realistic images. We have thus concentrated on volume-based surface rendering, which can compute images with a high grade of detail and realism. Although computing times for these volume-based methods are still longer than for triangular rendering, this disadvantage will be overcome by future hardware.

In our previous work, we developed a framework for volume-based anatomy atlases [22, 50]. One of the key procedures of this system is a high-quality volume rendering module, which uses volume-based ray casting methods. There are two conditions, that generally have to be fulfilled for the computation of high quality images:

1. The surface shading appears most realistic when the surface normals are determined by voxel intensity gradients [18, 57]. Thus the segmentation procedure, which precedes visualization, has to define the object borders "reasonably well" at the location of the intensity gradients.

2. The clusters defining an object in RGB space must be expressed in a simple analytical form in order to allow a fast refined classification of super-sampled data at ray casting time.

For scalar images (CT, MRI) these prerequisites are fulfilled by determination of an intensity range by a pair of lower and upper threshold values: First the threshold range yields object boundaries at the location of high intensity gradients, then the threshold can be interpolated in sub-voxel-resolution. The strong influence of the threshold specification on the rendering results is shown in figure 3.1: without threshold specification, surface locations can be computed in voxel resolution only, which leads to very blocky images. Using the threshold for super-sampling produces smooth surfaces, because the surface location is computed with very high accuracy.

For volume-based rendering of the Visible Human color images, the key problem for computation of high quality images is a generalization of scalar thresholds to a description in RGB-space. Pure enumeration of the RGB-tuples is not practical. The cluster should have a simple formal description for efficient computation during ray-casting. Attempts with a box-shaped classification in RGB space gave unsatisfactory results. Since objects in RGB space look rather ellipsoidal (see fig. 3.3) , we have decided to describe the classified regions by ellipsoids in RGB-space. For generalization of the scalar procedure for sub-voxel surface location, it is thus sufficient to find the point, where a straight line between two RGB-tuples intersects the ellipsoid (fig. 3.2). The required distance computations are done in Euclidean space with equal weights for all RGB-components.

In addition to the threshold generalization we have described, the visualization system has also been adapted in the following way to handle and take advantage of the Visible Human images:

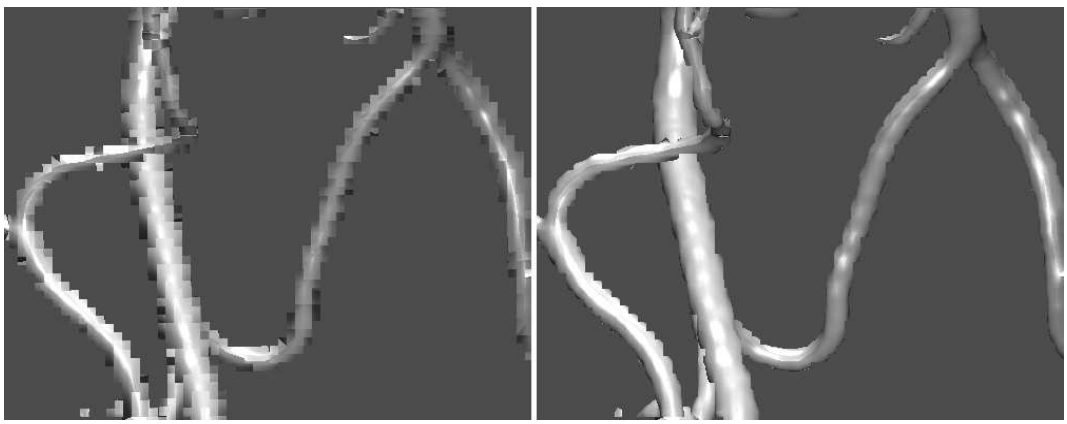

Figure 3.1: Influence of the threshold specification on the rendering result. Both images show a volume based rendering of the same voxel set. Left: Disregarding the threshold leads to blocky surfaces, because even super-sampling hits the voxel boundaries only. Right: Regarding the threshold during super-sampling produces a smooth and realistic surface appearance.

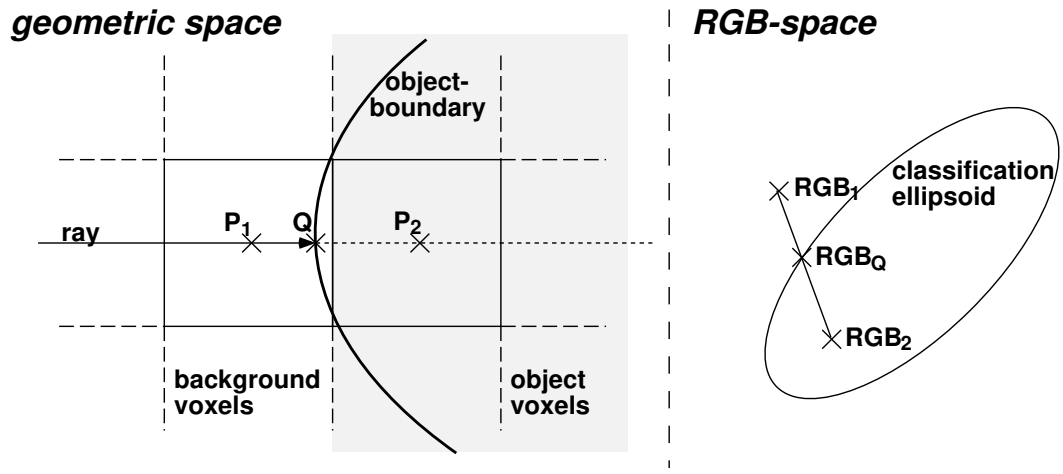

Figure 3.2: Using the ellipsoidal description of an object for sub-voxel computation of the surface location: Voxel P_2 with color RGB_2 carries the object label, voxel P_1 with color RGB_1 is outside the object to be visualized. The object surface is assumed to be at that point Q, which divides the line between P_1 and P_2 in the same ratio as RGB_Q divides RGB_1 and RGB_2.

- Instead of assigning an artificial color, texture mapping is performed by using the RGB-tuple at the surface location for the Phong illumination model.
- The surface normal is calculated as the normalized sum of the intensity gradients of each RGB-component.
- Rendering parameters can be taken from different data sets (anatomical, CT, or MRI) depending on the object (e.g. bone surface location and normal can be obtained from CT but the color from RGB

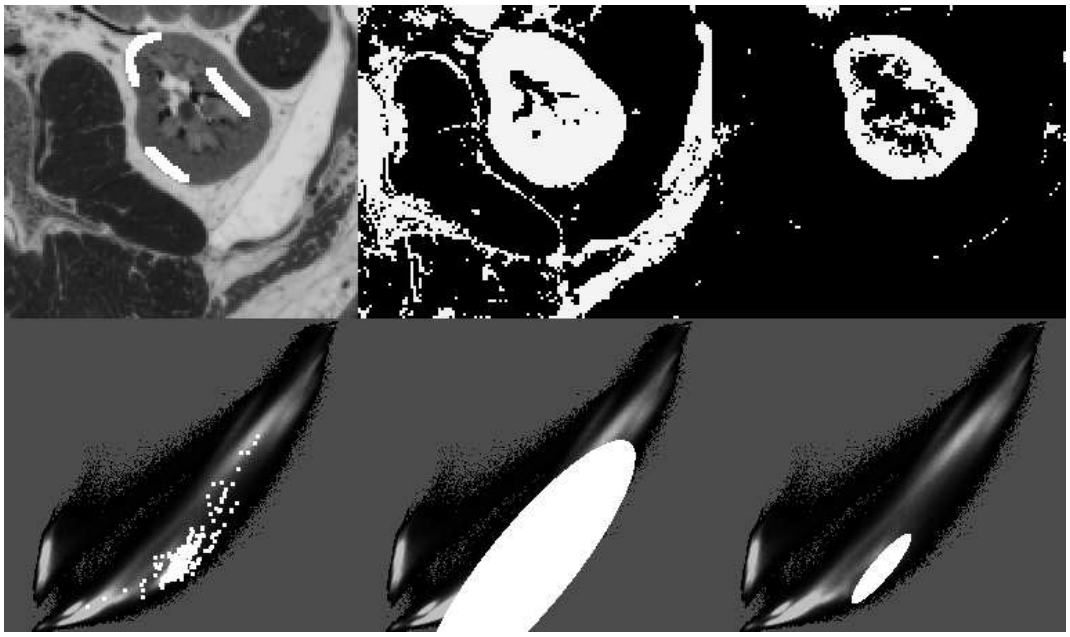

Figure 3.3: Interactive classification in RGB-space for the left kidney: The intermediate results are shown in the image space (upper row) and on 2D projections along the blue axis of the 3D scatter-plot (lower row). The user first outlines some typical areas of the kidney (left column). A preliminary result is obtained when all marked triples are used (middle). By restriction to the "substantial" triples, the final sharp classification is computed (right).

data). This option requires well registered data volumes, since misregistration leads to considerable artifacts.

3.2.3 Segmentation on basis of RGB-ellipsoids

Since the segmentation has to be done in great detail, an automatic segmentation is not possible and we aim instead at a semi-automatic procedure. The segmentation is adapted from an interactive method, which has proven to be successful for many purposes with scalar images like CT or MRI [21, 46]. The procedure is based on thresholding followed by binary mathematical morphology and connected component labeling. While the latter two steps remain unchanged for color images, the intensity range describing an object is replaced by an ellipsoid in RGB space. Determination of the ellipsoid is done by the following steps (fig. 3.3):

1. The users outlines a (usually small) typical region of the object to be segmented. This results in a set of color-triples $(RGB)_i$.

2. In most cases, the sample set $(RGB)_i$ will contain "wrong" triples, which belong to other structures, but have also been hit during outlining. In order to get rid of these triples, the median RGB-triple μ_{RGB} and the median μ_d of all Euclidean distances $d(\mu_{RGB} - (RGB)_i)$ are computed. For determination of the ellipsoid, only those triples closer to μ_{RGB} than an interactively specified multiple f of the median μ_d are further regarded.

3. The ellipsoid's center is taken from the median of the restricted sample set, the axes directions are

taken as the principal axes computed from covariance analysis, and the extent of the ellipsoid is determined such that all restricted triples are inside the ellipsoid.

During a practical session, the first goal is to define an ellipsoid that covers the object to be segmented. Due to the huge color feature space, several outlining steps will be necessary and "wrong"triples will be included in the ellipsoid (fig. 3.3 left). In this stage of the procedure, the multiple f is set to an upper limit, so that it has no further influence (fig. 3.3 middle). After that, the second goal is to refine the ellipsoid by reducing f (fig. 3.3 right). In our experiments, we ascertained that values between 2 and 4 are a good choice for f.

The problem of wrongly marked pixels in the first step is reduced significantly, if the full resolution (0.33 mm) images are used. This is due to the fact that the full resolution images show much sharper object boundaries, which can thus be more readily identified in the marking step. In addition, partial volume effects on the full resolution images are not very strong. Thus, the cluster of marked RGB-tuples is much sharper than that generated from images with reduced resolution.

Computing times for the ellipsoid itself are negligible, but for fast binary decision, if a triple is inside the ellipsoid or not, we use a binary volume of size 256^3, in which all triples inside the ellipsoid are set. Updating of this volume can take several seconds depending on the size of the ellipsoid.

The ellipsoidal classification in RGB-feature space is generally not sufficient for segmentation of an object without further processing steps in image space , because several structures are classified together. Connected component labeling and binary mathematical morphology are used to achieve further spatial decomposition of the voxels in the geometric space covered by the initial ellipsoid.

Instead of the proposed basic ellipsoidal specification, the segmentation step could also be performed with more sophisticated classification algorithms. However, for the method presented here, it is essential that all computations on the classification result be performed very quickly, because they are required several times for each image point during 3D rendering. Since more elaborated classification methods usually do not result in easily formalized descriptions (such as ellipsoids), these classification procedures cannot be used for our purpose.

The proposed segmentation procedure is successful for all major constituents of the body, such as the brain or abdominal organs. For a detailed subdivision of these structures, e.g. into gyri of the brain, manual segmentation is still needed, due to a lack of image properties for this purpose.

3.3 Results

Although the availability of the Visible Human images is rather recent, a number of systems for their exploration does already exist. Unfortunately, most of these systems present the images only as stacks of orthogonal slices, which can be browsed through with different techniques. The number of real 3D applications [24, 53] is still limited.

We have applied our method to several regions of the Visible Human male (fig. 3.4). The major constituents of the head, the upper abdomen, and the right shoulder have been segmented with the interactive segmentation procedure described above. Most structures (e.g. brain, kidneys, muscles, intestine) can be segmented in a few minutes on a workstation DEC 3000 with 256 M-byte of main memory. Extended organs like the liver with many links to other structures need additional interaction on single slice sequences.

The main areas of application for techniques using the Visible Human datasets are teaching (especially in anatomy and radiology) and simulation. Figure 3.5 gives an example of a typical teaching image showing a view of the upper abdomen with kidneys, spleen, muscles, vertebral column, and abdominal vasculature. The cut planes show the anatomical colors of the underlying data volume. Texture mapping

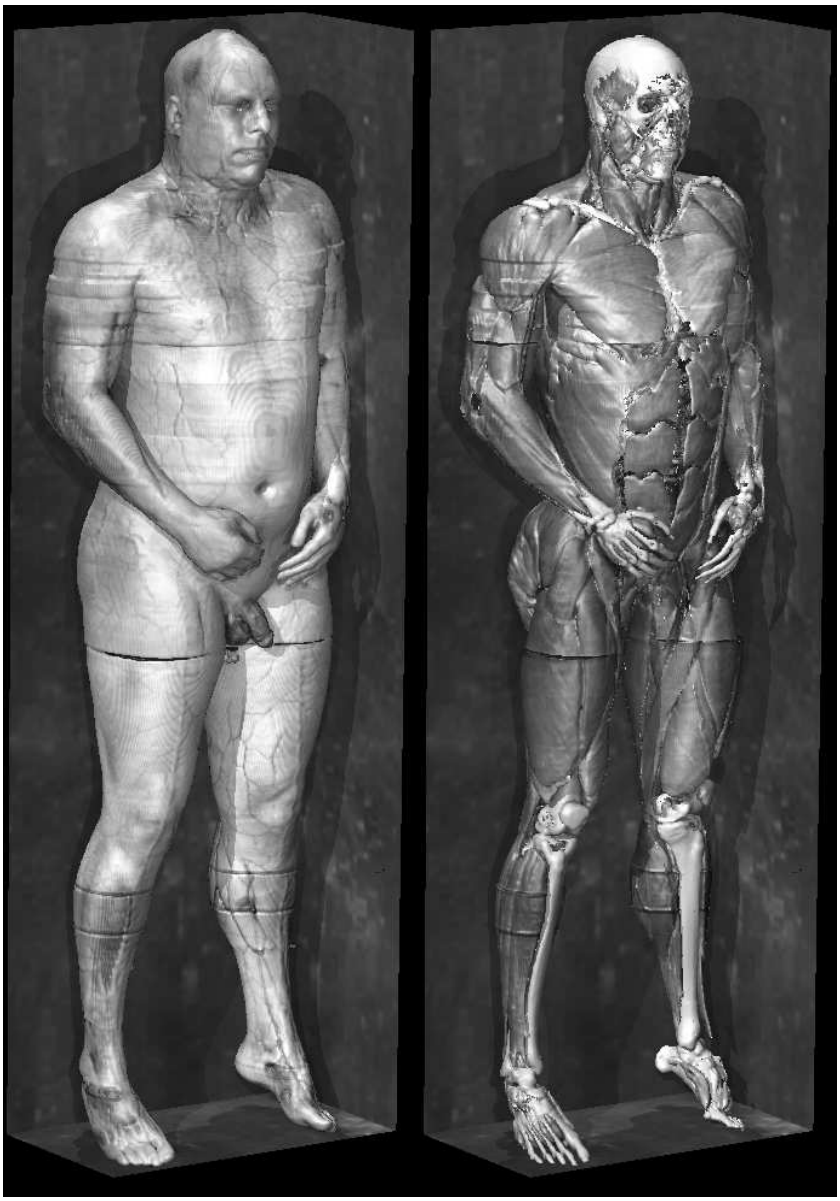

Figure 3.4: Views of the Visible Human Male: Skin surface, and bone and muscles.

of the anatomical colors is used for shading of most 3D rendered structures, while for bone and blood vessels, artificial colors are chosen in order to enhance their appearance.

Figure 3.6 shows a view of the muscles of the right shoulder, which have been segmented from the anatomical data. The bone structures have been segmented from the frozen CT data. Texture mapping is not performed for the bone, but an artificial color is again chosen for enhancement. The shoulder region is hit by several shift artifacts, which are visible as horizontal lines.

The possibility of simulation is shown with the example of virtual endoscopy (fig. 3.7). From a perspective inside the stomach pictures resembling those obtained during real gastroscopy are generated with realistic

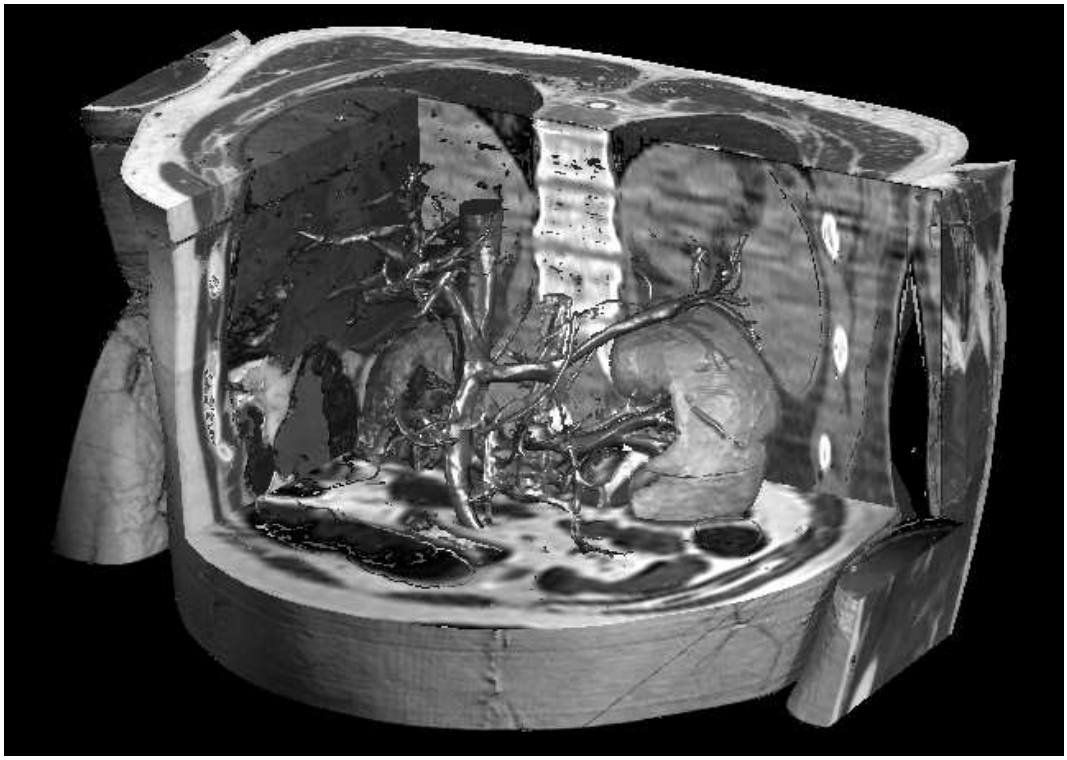

Figure 3.5: Abdominal anatomy as obtained with the interactive segmentation procedure. Some objects (vasculature, bone) are colored artificially for better distinction.

colors and great anatomical detail.

Further 3D renderings of the Visible Human's head and abdomen have been published elsewhere [48, 58].

3.4 Conclusion

We have proposed a new combined approach of interactive classification and volume-based visualization of RGB volumes such as those of the Visible Human. The pictures show that the rendering quality obtained with the method described here is superior to that of other approaches published so far.

Our first steps in segmentation for high resolution volume rendering show that the Visible Human data set allows a new quality of anatomical imaging when used in a state-of-the-art visualization system. Nevertheless, a huge amount of work still has to be done to achieve detailed segmentation necessary for a complete 3D anatomical atlas. But unlike clinical imaging, which requires new segmentation for every case, segmentation of the Visible Human has to be done only once. If this work is completed, the results will surely have great impact on many applications of visualization such as education and simulation.

3.5 Acknowledgements

We are grateful to all the members of our department who have supported this work. Special thanks to Rainer Schubert for anatomical and Uwe Pichlmeier for statistical support. Our thanks go also to

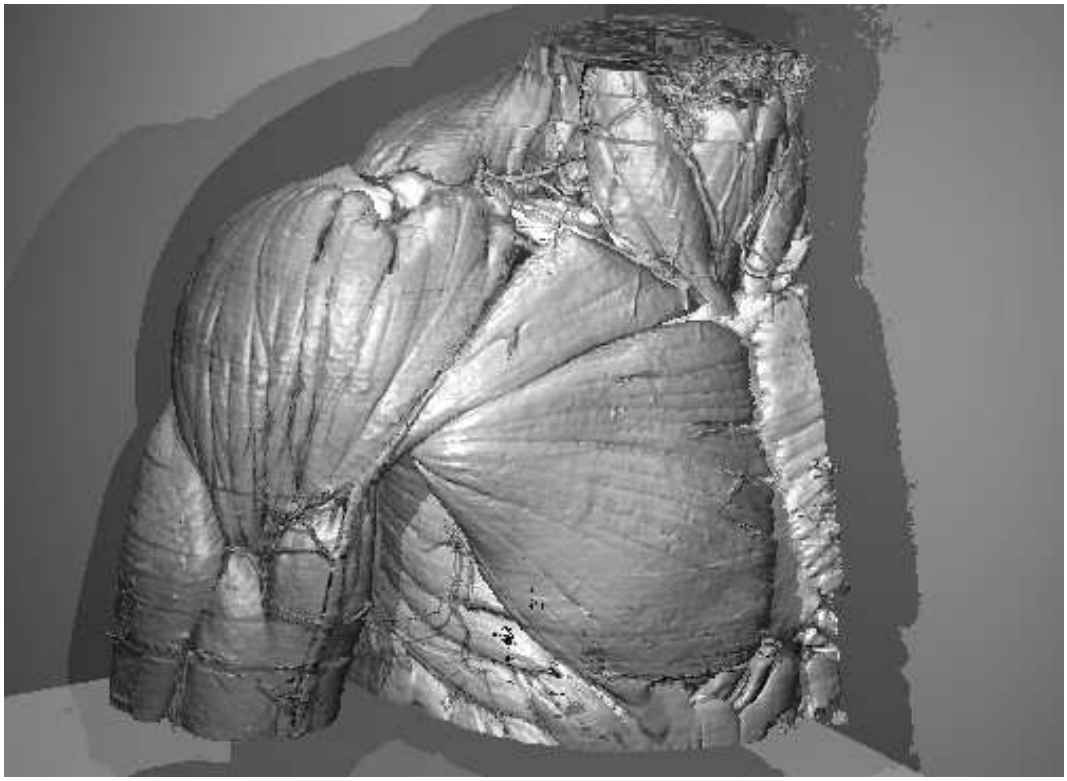

Figure 3.6: The Visible Human's right shoulder. Photo-realistic quality is achieved exhibiting even small vessels.

Victor Spitzer, University of Colorado School of Medicine, and Michael Ackerman, National Library of Medicine, for providing the Visible Human data set.

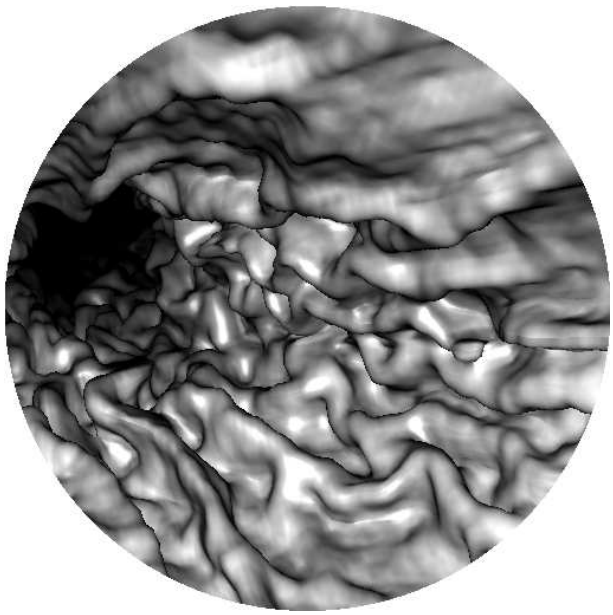

Figure 3.7: Simulation of gastroscopy showing the typical surface structures of the stomach.

Bibliography

[1] Ackerman, M. J.: Viewpoint: The Visible Human project. *J. Biocommun. 18* (1991), 14.

[2] Bernauer, J.: Analysis of part-whole relation and subsumption in the medical domain. *Data Knowl. Eng. 20* (1996), 405–415.

[3] Bloom, F. E.: Databases of brain information. In Toga, A. W. (Ed.): *Three-Dimensional Neuroimaging*, Raven Press, New York, 1990, ch. 13, 273–306.

[4] Bookstein, F.: *Morphometric Tools for Landmark Data.* Cambridge University Press, New York, 1991.

[5] Brechbühler, C., Gerig, G., Kübler, O.: Surface Parametrisation and Shape Description. In *Proc. First Conference on Visualization in Biomedical Computing, VBC '92.* Chapel Hill, 1992, 80–89.

[6] Brinkley, J. F., Eno, K., Sundsten, J. W.: Knowledge-based client-server approach to structural information retrieval: The Digital Anatomist Browser. *Comput. Methods Programs Biomed. 40*, 2 (1993), 131–145.

[7] Brinkley, J. F., Rosse, C.: The Digital Anatomist distributed framework and its applications to knowledge-based medical imaging. *J. Am. Med. Inf. Ass. 4*, 3 (1997), 165–183.

[8] Carlsen, I. C., Imme, M., Kuhn, M. H., Menhardt, W., Ottenberg, K., Schmidt, K. H.: Knowledge Based Interpretation of Cranial MR Images. In Lemke, H. U. et al. (Eds.): *Computer Assisted Radiology, Proc. CAR '91.* Springer-Verlag, Berlin, 1991, 277–282.

[9] Côté, R. A. (Ed.): *SNOMED—Systematized Nomenclature of Medicine.* 2. ed. College of American Pathologists, Skokie, IL, 1979.

[10] Declerck, J., Subsol, G., Thirion, I., Ayache, N.: Automatic Retrieval of Anatomical Stuructures in 3D Medical Images. In *Proc. First International Conference on Compter Vision, Virtual Reality and Robotics in Medicine, CVRMed.* Nice, 1995, 153–162.

[11] Dev, P., Coppa, G. P., Tancred, E.: BrainStorm: Designing an Interactive Neuroanatomy Atlas. *Radiology 185 (P)* (1992), 413. (abstract).

[12] Drebin, R. A., Carpenter, L., Hanrahan, P.: Volume rendering. *Comput. Graphics 22*, 4 (1988), 65–74.

[13] Evans, A. C., Beil, C., Marret, S., et al.: Anatomical-functional correlation using an adjustable MRI-based region of interest atlas with positron emission tomography. *J. Cereb. Blood Flow Metab. 8*, 4 (1988), 513–530.

[14] Fox, P. T., Mikiten, S., Davis, G., Lancaster, J. L.: BrainMap: A database of human functional brainmapping. In Thatcher, R. W. et al. (Eds.): *Functional Neuroimaging: Technical Foundations*, Academic Press Inc., Orlando, FL, 1994, ch. 9, 95–105.

[15] Gee, J. C., Reivich, M., Bajcsy, R.: Elastically deforming a 3D atlas to match anatomical brain images. *J. Comput. Assist. Tomogr. 17*, 2 (1993), 225–236.

[16] Greitz, T., Bohm, C., S., Holte, Eriksson, L.: A computerized brain atlas: Construction, anatomical content, and some applications. *J. Comput. Assist. Tomogr. 15*, 1 (1991), 26–38.

[17] Höhne, K. H. (Ed.): *VOXEL-MAN Junior: Interactive 3D Anatomy and Radiology in Virtual Reality Scenes, Part 1: Brain and Skull.* Springer-Verlag Electronic Media, Heidelberg, 1998. (CD-ROM, ISBN 3-540-14676-8).

[18] Höhne, K. H., Bernstein, R.: Shading 3D-images from CT using gray level gradients. *IEEE Trans. Med. Imaging MI-5*, 1 (1986), 45–47.

[19] Höhne, K. H., Bomans, M., Pommert, A., Riemer, M., Schiers, C., Tiede, U., Wiebecke, G.: 3D-visualization of tomographic volume data using the generalized voxel-model. *Visual Comput. 6*, 1 (1990), 28–36.

[20] Höhne, K. H., Bomans, M., Riemer, M., Schubert, R., Tiede, U., Lierse, W.: A 3D anatomical atlas based on a volume model. *IEEE Comput. Graphics Appl. 12*, 4 (1992), 72–78.

[21] Höhne, K. H., Hanson, W. A.: Interactive 3D-segmentation of MRI and CT volumes using morphological operations. *J. Comput. Assist. Tomogr. 16*, 2 (1992), 285–294.

[22] Höhne, K. H., Pflesser, B., Pommert, A., Riemer, M., Schiemann, T., Schubert, R., Tiede, U.: A new representation of knowledge concerning human anatomy and function. *Nature Med. 1*, 6 (1995), 506–511.

[23] Höhne, K. H., Pommert, A., Riemer, M., Schiemann, T., Schubert, R., Tiede, U., Lierse, W.: Framework for the generation of 3D anatomical atlasses. In Robb, R. A. (Ed.): *Visualization in Biomedical Computing II, Proc. SPIE 1808.* Chapel Hill, NC, 1992, 510–520.

[24] Hong, L., Kaufman, A., Wei, Y.-C., Viswambharan, A., Wax, M., Liang, Z.: 3D Virtual Colonoscopy. In *IEEE Biomedical Visualization Symposium.* 1996, 26–32.

[25] IMDM: VOXEL-MAN brain and skull. Springer Electronic Media. Heidelberg New York, 1995.

[26] International Anatomical Nomenclature Committee (Ed.): *Nomina Anatomica.* 6. ed. Churchill Livingstone, Edinburgh, 1989. (Together with Nomina Histologica, 3. ed., and Nomina Embryologica, 3. ed.).

[27] Kaufman, A. (Ed.): *Volume Visualization.* IEEE Computer Society Press, Los Alamitos, CA, 1991.

[28] Keyserlingk, D. G., Niemann, K., Wasel, J., Maurer, K.: Digital brain atlas for structure localization in CT combined with EEG mapping. *Psychiatry Res. 29*, 3 (1989), 461–462.

[29] Lehmann, E. D., Hawkes, D. J., Hill, D. L., Bird, C. F., Robinson, G. P., Colchester, A. C., Maisey, M. N.: Computer-aided interpretation of SPECT images of the brain using an MRI-derived 3D neuro-anatomical atlas. *Med. Inform. 16*, 2 (1991), 151–166.

[30] Levoy, M.: Display of surfaces from volume data. *IEEE Comput. Graphics Appl. 8*, 3 (1988), 29–37.

[31] Lipscomb, K., Kittrel, A.: Software gets under your skin. *Physicians and Computers 9*, 7 (1991), 14–16.

[32] Lorensen, W. E., Cline, H. E.: Marching Cubes: A high resolution 3D surface construction algorithm. *Comput. Graphics 21*, 4 (1987), 163–169.

[33] Mano, I., Suto, Y., Suzuki, M., Iio, M.: Computerized three-dimensional normal atlas. *Radiat. Med. 8*, 2 (1990), 50–54.

[34] Menhardt, W.: Iconic fuzzy sets for MR image segmentation. In Todd-Pokropek, A. E., Viergever, M. A. (Eds.): *Medical Images: Formation, Handling and Evaluation*, NATO ASI Series F 98, Springer-Verlag, Berlin, 1992, 579–591.

[35] Natarajan, K., Claridge, E., Davis, D. N.: The symbolic atlas of the brain: Handling non-visual information associated with neuroanatomy. *Med. Inform. 21*, 1 (1996), 1–22.

[36] Ney, D., Fishman, E. K., Magid, D., Robinson, D. D., Kawashima, A.: Three-dimensional volumetric display of CT data: effect of scan parameters upon image quality. *J. Comput. Assist. Tomogr. 15* (1991), 875–885.

[37] Niemann, H., Sagerer, G. F., Schröder, S., Kummert, F.: ERNEST: A semantic network system for pattern understanding. *IEEE Trans. Pattern Anal. Machine Intell. 12*, 9 (1990), 883–905.

[38] Niemann, K., Keyserlingk, D. G. v., Wasel, J.: Superimposition of an Averaged Three-Dimensional Pattern of Brain Structures on CT Scans. *Acta Neurochir. 93* (1988), 61–67.

[39] Pflesser, B., Tiede, U., Höhne, K. H.: Specification, modelling and visualization of arbitrarily shaped cut surfaces in the volume model. In Grimson, W. E. L. (Ed.): *Medical Image Computing and Computer-Assisted Intervention, Proc. MICCAI '98*. Cambridge, MA, 1998. (accepted for publication).

[40] Pommert, A., Bomans, M., Höhne, K. H.: Volume visualization in magnetic resonance angiography. *IEEE Comput. Graphics Appl. 12*, 5 (1992), 12–13.

[41] Pommert, A., Riemer, M., Schiemann, T., Schubert, R., Tiede, U., Höhne, K. H.: Knowledge-based and 3D imaging systems in medical education. In Brunnstein, K., Raubold, E. (Eds.): *Information Processing '94, Proc. IFIP 13. World Computer Congress, Vol. II: Applications and Impacts*, IFIP Transactions A-52, North-Holland, Amsterdam, 1994, 525–532.

[42] Pommert, A., Schubert, R., Riemer, M., Schiemann, T., Tiede, U., Höhne, K. H.: Symbolic modeling of human anatomy for visualization and simulation. In Robb, R. A. (Ed.): *Visualization in Biomedical Computing 1994, Proc. SPIE 2359*. Rochester, MN, 1994, 412–423.

[43] Robinson, G. P., Colchester, A. C. F., Griffin, L. D.: Model-based recognition of anatomical objects from medical images. *Image and Vision Computing 12*, 8 (1994), 499–507.

[44] Rosse, C., Said, M. B., Eno, K. R., Brinkley, J. F.: Enhancements of anatomical information in UMLS knowledge sources. In *Annu. Symp. Comput. Appl. Med. Care, Proc. SCAMC*. New Orleans, LA, 1995, 873–877.

[45] Schaltenbrand, G., Wahren, W.: *Atlas for stereotaxy of the human brain*. Thieme, Stuttgart, 1977.

[46] Schiemann, T., Bomans, M., Tiede, U., Höhne, K. H.: Interactive 3D-segmentation. In Robb, R. A. (Ed.): *Visualization in Biomedical Computing II, Proc. SPIE 1808*. Chapel Hill, NC, 1992, 376–383.

[47] Schiemann, T., Höhne, K. H., Koch, C., Pommert, A., Riemer, M., Schubert, R., Tiede, U.: Interpretation of tomographic images using automatic atlas lookup. In Robb, R. A. (Ed.): *Visualization in Biomedical Computing 1994, Proc. SPIE 2359*. Rochester, MN, 1994, 457–465.

[48] Schiemann, T., Nuthmann, J., Tiede, U., Höhne, K. H.: Generation of 3D anatomical atlases using the Visible Human. In Kilcoyne, R. F. et al. (Eds.): *Computer Applications to Assist Radiology, Proc. SCAR '96*, Symposia Foundation, Carlsbad, CA, 1996, 62–67.

[49] Schubert, R., Höhne, K. H.: Partonomies for interactive explorable 3D-models of anatomy. In *American Medical Informatics Association, Proc. AMIA '98*. Orlando, FL, 1998. (to be published).

[50] Schubert, R., Höhne, K. H., Pommert, A., Riemer, M., Schiemann, T., Tiede, U.: Spatial knowledge representation for visualization of human anatomy and function. In Barrett, H. H., Gmitro, A. F. (Eds.): *Information Processing in Medical Imaging, Proc. IPMI '93*, Lecture Notes in Computer Science 687, Springer-Verlag, Berlin, 1993, 168–181.

[51] Schubert, R., Höhne, K. H., Pommert, A., Riemer, M., Schiemann, T., Tiede, U., Lierse, W.: A new method for practicing exploration, dissection, and simulation with a complete computerized three-dimensional model of the brain and skull. *Acta Anat. 150*, 1 (1994), 69–74.

[52] Schulz, S., Romacker, M., Hahn, U.: Part-whole reasoning in medical ontologies revisited: A classification-based description logic perspective. In *American Medical Informatics Association, Proc. AMIA '98*. Orlando, FL, 1998. (to be published).

[53] Seymour, J.: A New 3D Database and Atlas Based on the Visible Human. In *Second Southeastern Medical Informatics Conference*. Gainsville, FL, 1996.

[54] Spitzer, V., Ackerman, M. J., Scherzinger, A. L., Whitlock, D.: The Visible Human male: A technical report. *J. Am. Med. Inf. Ass. 3*, 2 (1996), 118–130.

[55] Talairach, J., Tournoux, P.: *Co-planar stereotaxic atlas of the human brain*. Thieme, Stuttgart, 1988.

[56] Tiede, U., Bomans, M., Höhne, K. H., Pommert, A., Riemer, M., Schiemann, T., Schubert, R., Lierse, W.: A computerized three-dimensional atlas of the human skull and brain. *Am. J. Neuroradiology 14*, 3 (1993), 551–559.

[57] Tiede, U., Höhne, K. H., Bomans, M., Pommert, A., Riemer, M., Wiebecke, G.: Investigation of medical 3D-rendering algorithms. *IEEE Comput. Graphics Appl. 10*, 2 (1990), 41–53.

[58] Tiede, U., Schiemann, T., Höhne, K. H.: Visualizing the Visible Human. *IEEE Comput. Graphics Appl. 16*, 1 (1996), 7–9.

[59] Wahler-Lück, M., Schütz, T., Kretschmann, H.-J.: A new anatomical representation of the human visual pathways. *Graefe's Arch. Clin. Exp. Ophthalmol. 229*, 3 (1991), 201–205.

[60] Wertheim, S. L.: The brain database: a multimedia database for neuroscience research and teaching. *Annu. Symp. Comput. Appl. Med. Care, Proc. SCAMC 13* (1989), 399–404.

[61] Winston, P. H.: *Artificial Intelligence*. 3. ed. Addison-Wesley, Reading, MA, 1992.